Engineering and Technology Journal
Journal homepage: https://etj.uotechnology.edu.iq

Enhancing wind tunnel computational simulations of finite element analysis using machine learning-based algorithms

Luttfi A. Al-Haddad[a]*, Alaa A. Jaber[b], Latif Ibraheem[c], Sinan A. Al-Haddad[d], Naseem S. Ibrahim[a], Fawaz M. Abdulwahed[a]

[a] Training and Workshops Center, University of Technology-Iraq, Alsina'a street, 10066 Baghdad, Iraq.
[b] Mechanical Engineering Dept., University of Technology-Iraq, Alsina'a street, 10066 Baghdad, Iraq.
[c] Mechanical Engineering Dept., Memorial University of Newfoundland, Newfoundland and Labrador, Canada.
[d] Civil Engineering Dept., University of Technology-Iraq, Alsina'a street, 10066 Baghdad, Iraq.
*Corresponding author Email: Luttfi.A.AlHaddad@uotechnology.edu.iq

HIGHLIGHTS

- A Finite Element Analysis, of an Aircraft model in a wind tunnel using ANSYS Fluent and Structural Analysis, is presented
- Artificial Intelligence-based machine learning models are presented, namely SVM and kNN regression models
- The stress distribution on the aircraft front wing is predicted by Machine Learning models, and RMSE compared their accuracy

ARTICLE INFO

Handling editor: Jalal M. Jalil
Keywords:
Finite element analysis
Machine learning
Wind tunnel
Stress distribution
Deformation

ABSTRACT

Wind tunnels are essential for examining aircraft model aerodynamics, accurately simulating real-world conditions, and enhancing design and performance evaluations. This study introduces a novel technique to improve the time and accuracy of stress distribution forecasts in wind tunnel simulations. This method combines Finite Element Analysis (FEA) with two regression models: Support Vector Machine (SVM) and k-Nearest Neighbors (kNN). The investigation begins with a thorough analysis of ANSYS fluent flow data, which reveals intricate fluid dynamics details within the wind tunnel. A comparative analysis of stress projections, supplemented by Root Mean Square Error (RMSE) metric, demonstrates the proposed methodology's viability. High accuracy is noted in the SVM-based model, as evidenced by its 2.1% RMSE, which surpasses the kNN model's 5.6% RMSE. Notably, the stress distribution calculation took almost 2 hours in ANSYS.In contrast, it required only 10 seconds in SVM and 3 seconds in kNN, showcasing the time-efficient attributes of these models where they solely depend on the trained data. Moreover, the computational efficacy of the SVM and kNN models is highlighted, emphasizing their flexibility in stress analysis. This integrative approach introduces a promising potential in engineering simulations, yielding precise stress distribution forecasts that have the potential to advance aircraft design methodologies and wind tunnel evaluations.

1. Introduction

The field of aeronautics consistently aims for innovation and progress to enhance the safety, effectiveness, and overall performance of aircraft Al-Haddadet al. [1], Al-Haddadet al., [2]. Comprehending how tension is distributed across a model during wind tunnel tests holds significant importance for aircraft design and operations Cui et al. [3], Westin et al., [4]. The field of aerospace engineering continues to depend heavily on wind tunnel testing as a means to conduct comprehensive examinations of aerodynamics and structural performance inside controlled environments Smolka et al. [5], Chen et al., [6]. In this context, precise examination of stress distribution plays a pivotal role in guaranteeing the structural robustness and optimal functionality of aircraft Li et al., [7].

This research aims to explore a unified approach that combines Finite Element Analysis (FEA) with Artificial Intelligence (AI) to enhance the precision of stress distribution forecasts for aircraft models within wind tunnel simulations. In this context, machine learning-based models Al-Haddad and Jaber [8], namely support vector machine and k nearest neighbor, will be adopted instead of time-consuming simulations. For decades, FEA has been a foundational tool across engineering disciplines, enabling engineers to replicate complex structural behaviors by breaking them down into manageable elements Al-Haddad and Jaber [9], Shijer [10], Dubaish and Jaber [11], Yassa et al., [12]. Nevertheless, with the escalating complexity of designs and analyses, there arises a necessity to explore supplementary methodologies that ensure precise predictions and, notably, curtail simulation

http://doi.org/10.30684/etj.2023.142873.1552
Received 28 August 2023; Received in revised form 28 September 2023; Accepted 7 October 2023; Available online 15 November 2023
2412-0758/University of Technology-Iraq, Baghdad, Iraq

durations. In recent times, the emergence of Artificial Neural Networks (ANNs) has brought about a transformative shift in tackling intricate challenges Al-Haddad et al., [13]. The capacity of machine learning-driven models to assimilate intricate associations from data renders them highly suitable for tasks involving pattern recognition and predictive capabilities Casabianca and Zhang [14], Xiaoqian [15], Moussafir et al., [16]. The convergence of FEA and machine learning engenders an avenue to amplify predictions encompassing stress distribution and geometry deformation, capitalizing on the distinctive strengths of both methodologies.

This study aims to showcase how the fusion of FEA with regression models can yield a more precise stress distribution model for aircraft models subjected to wind tunnel assessments with an extremely shorter amount of time. The initial phase of FEA pertains to fluid flow simulations executed within ANSYS Fluent. In contrast, the subsequent phase involves static structural analysis for stress computations facilitated by incorporating regression models. This approach underscores the latent benefits of integrating artificial intelligence to enhance traditional engineering evaluations.

2. Finite element analysis

FEA stands as a foundational methodology in the arsenal of engineers, particularly in the realm of structural engineering and simulation. It serves as a pivotal approach for dissecting and forecasting intricate behaviors exhibited by intricate structures when subjected to a myriad of loading conditions Ogaili et al., [17] Flaieh et al., [18]. The significance of FEA derives from its capacity to provide a systematic and computationally efficient framework for comprehending essential mechanical traits such as stress distribution and deformation. Through the dissection of intricate systems into discrete components, a comprehensive understanding of localized behaviors is attained, thereby fostering optimization of designs and enhancement of structural integrity. This section immerses into the fundamental underpinnings of FEA and its application in the context of aircraft models within wind tunnel simulations. The procedure encompassing the generation of finite element models, specification of material attributes, and imposition of boundary conditions to mimic real-world scenarios is delineated step by step. Moreover, an in-depth exploration of the advantages and limitations of FEA is undertaken, paving the way for a profound grasp of its role as the bedrock of the integrated methodology.

2.1 Computer-aided design

The use of computer-aided design (CAD) has significantly revolutionized the field of engineering by enabling the creation, alteration, and evaluation of intricate designs inside a simulated environment Chang [19]. CAD is pivotal in wind tunnel simulations as it generates meticulous geometric representations of the wind tunnel and the aircraft prototype model. The wind tunnel exhibits a length of 3 meters and a cross-sectional dimension of 0.8 meters by 0.8 meters, as illustrated in Figure 1a. This configuration constructs a controlled testing milieu that facilitates precise scrutiny of airflow dynamics and structural responses. Figure 1b elucidates the precise measurements of the aircraft prototype model in millimeters, which will be subjected to ANSYS simulations. These dimensions furnish the groundwork for subsequent finite element investigations and stress distribution prognostications, pivotal for validating the model's performance and ensuring its safety within the wind tunnel. Additionally, it's imperative to underline that the inlet is subjected to a boundary condition of 5m/s² while a pressure outlet is elected.

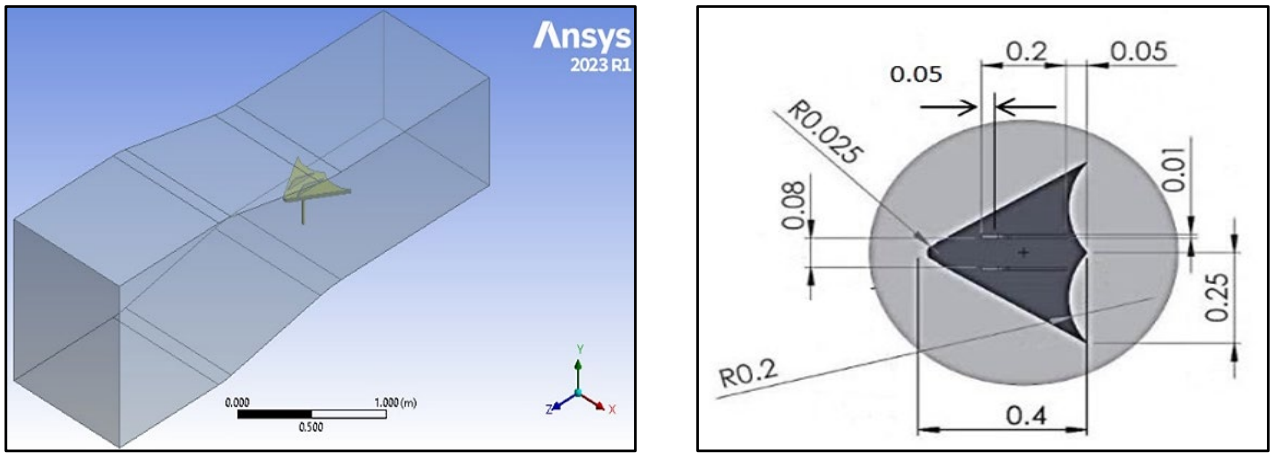

(a) (b)

Figure 1: Geometrical approach: (a) Geometry of wind tunnel, (b) Geometry of aircraft model

2.2 Computer-aided engineering

The landscape of engineering analysis has been revolutionized by Computer-Aided Engineering (CAE), equipping engineers with robust tools to realistically simulate and assess intricate systems. Within this context, ANSYS software emerges as a cornerstone of CAE methodologies, enabling the seamless amalgamation of fluid dynamics and structural analysis to comprehensively explore the intricate interplay between aerodynamics and structural integrity. As depicted in Figure 2, the simulation process epitomizes a harmonious collaboration between ANSYS Fluent, specializing in fluid flow analysis, and ANSYS Mechanical, adept at static structural analysis. This conjunction facilitates an all-encompassing scrutiny of the intricate

nexus between aerodynamic forces and the consequential stress distribution on the aircraft prototype model. Through this symbiotic simulation strategy, a heightened comprehension of how fluid flow impacts the structural behavior of the model is achieved, thus paving the way for enhanced accuracy in stress prediction.

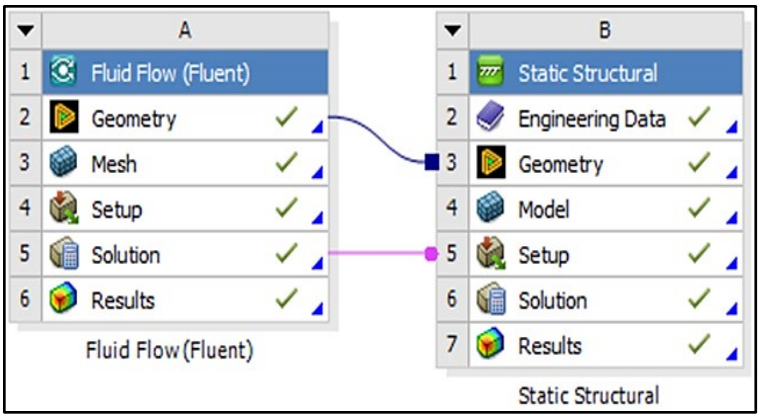

Figure 2: ANSYS program widgets

3. Machine learning models

3.1 Support vector machine

SVM, an abbreviation for Support Vector Machine, constitutes a machine learning framework operating within a statistical learning paradigm, catering to classification and regression undertakings. The architecture of this aforesaid entity is rooted in establishing hyperplanes within a space characterized by high or infinite dimensions, thereby facilitating a heightened level of generality. As depicted in Figure 3, the fundamental tenet of SVM revolves around identifying an optimal hyperplane within the feature space to demarcate datasets effectively. In the illustration, the classification boundary is represented as H, accompanied by two parallel lines denoted H_1 and H_2, which traverse the data points nearest to H from the respective data types. These data points find expression as support vectors, while the gap between H_1 or H_2 and H signifies the geometric separation. Consequently, the primary objective of SVM training hinges on maximizing this geometric margin.

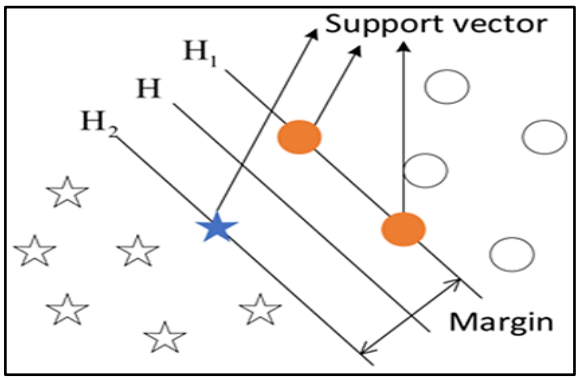

Figure 3: SVM algorithm illustration [20]

The optimization function integrates a regularization parameter to counteract overfitting concerns. Furthermore, utilizing a convex function is instrumental in circumventing the potential stumbling block of encountering local minima facilitated by proficient methodologies. Within the ambit of support vector regression, the Kernel function assumes a pivotal role, and it can manifest in three distinct types: linear, polynomial, or radial basis function (RBF) Al-Mukhtar [21]. The RBF is expressed by Equation 1 below Al-Mukhtar [22]. Here, x and y represent different dosage measurements of arbitrary inputs. Determining the value of g is achievable via cross-validation, a process that duly magnifies its influence, and this value is automatically established.

$$Kernal = e^{-g|x-y|^2} \quad (1)$$

- Kernel function: Denoted as $K(x, y)$, similarity or dissimilarity between two data points, x, and y, is measured by it.
- e: The base of the natural logarithm, approximately equal to 2.71828, is used; it's a mathematical constant.
- g $(gamma)$: A parameter in the Gaussian RBF kernel controls the shape of the kernel function. A positive constant determines the width and complexity of the curve.
  Now, let's explain the function's operation:
- When the kernel function is applied to two data points, x and y, the Euclidean distance between them, $|x - y|$, is computed.

- This distance is squared, yielding. $|x - y|^2$.
- The presence of the negative sign in front of gamma (-g) implies that the resulting value will decrease exponentially as the distance between x and y increases. Consequently, the kernel function assigns a high value to data points that are close (i.e., similar) and a low value to those that are far apart (i.e., dissimilar).
- The exponential term $e^{-g|x-y|^2}$ further amplifies this behavior, making the measure of similarity/dissimilarity highly sensitive to the spatial separation between data points. This heightened sensitivity, facilitated by the Gaussian RBF kernel, effectively captures intricate data relationships.

The essence of SVM's operation involves mapping data into a high-dimensional subspace, enabling the classification of data points that might otherwise lack differentiation. A separator is unveiled between the distinct categories, and the data undergo manipulation to facilitate the depiction of this separator as a hyperplane. The parameters of the proposed model are outlined in Table 1.

Table 1: Parameters of the proposed SVM classification model

Data	Value
Cost	1.02
Regression loss epsilon	0.09
Kernal	RBF
Iteration limit	200

The important parameters of the proposed SVM classification model are shown in Table 1. These parameters are critical in determining how the SVM algorithm works and how well it executes the classification job. Let us go through each parameter:

- Cost: In SVM, the cost parameter (C) specifies the trade-off between increasing the margin (distance between decision border and support vectors) and reducing classification errors. The value of C is set to 1.02 in this situation. A higher C value causes the model to prioritize correct training data point categorization, possibly resulting in a tighter margin. In comparison, a lower C value prioritizes a broader margin, tolerating some misclassification.
- Regression Loss Epsilon: In SVM regression tasks, this parameter, designated as epsilon, is employed. It specifies a tolerance range within which no penalty is imposed for mistakes. The epsilon value in this classification model is set at 0.09. This indicates that any classification mistake within this margin is accepted, and only errors outside this limit are punished.
- The kernel function controls the data transformation, enabling SVM to locate non-linear decision boundaries in a higher-dimensional feature space. The Radial Basis Function (RBF) kernel was chosen in this scenario because of its efficacy in capturing complicated correlations in data.
- Iteration Limit: The iteration limit determines the maximum number of iterations or optimization steps the SVM algorithm performs during training. The iteration limit in this model is set to 200, which means that the algorithm will cease optimizing after this number of iterations.

These parameters determine the SVM classification model's behavior and performance as a whole. The values for these parameters are determined depending on the issue's features, and they may be fine-tuned via experimentation to produce the best classification results for the current dataset and job

3.2 K nearest neighbor

The k-nearest neighbors (kNN) method is a straightforward and intuitive technique in supervised machine learning. It is proficient at handling classification and regression tasks. The setup procedure is characterized by its simplicity and ease of understanding. Nevertheless, one notable limitation of this methodology is its decreased velocity when the quantity of employed data expands. The methodology produces positive results regarding visual and numerical classification precision. Figure 4 illustrates the procedural steps involved in the k-nearest neighbors (kNN) method, while Table 2 presents the specific parameters used in the model suggested. The primary goal is to maximize efficiency while decreasing the time required for completion.

Table 1: Specifications of the kNN model

Data	Value
Number of Neighbors	6
Metric	Manhattan
Weight	Distance

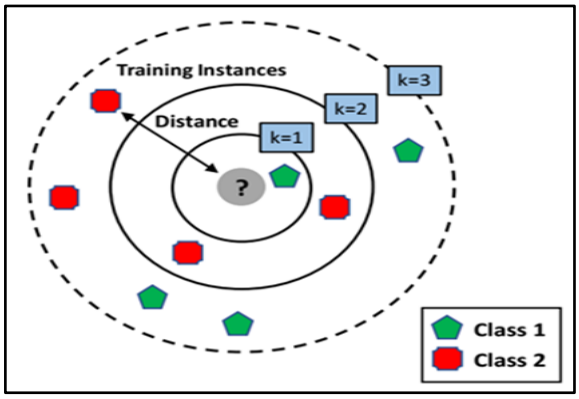

Figure 4: kNN algorithm illustration [23]

As previously indicated in Table 2, the kNN algorithm employs diverse distance calculation approaches, encompassing Euclidean and Manhattan distances, to gauge the likeness or nearness between two data points. Among these methodologies, the Euclidean distance enjoys broad application and can be articulated mathematically through the ensuing Equation 2:

$$D(X,Y) = \sqrt{\sum_{i=1}^{n}(x_i - y_i)^2} \quad (2)$$

The expression representations:

- $D(X,Y)$: This represents the Euclidean distance between two vectors, X and Y.
- $X = (x_1, x_2, x_3, \ldots, x_n)$: X is an n-dimensional vector with n components or features.
- $Y = (y_1, y_2, y_3, \ldots, y_n)$: Y is another n-dimensional vector with the same number of components.

Now, to explain the formula:

- $(x_i - y_i)$: This calculates the difference between the corresponding components of X and Y for each i from 1 to n.
- $\sum_{i=1}^{n}(x_i - y_i)^2$: This squares each of these differences.
- $\sum(x_i - y_i)^2$: This symbol ($\sum$) represents the summation, which means adding up all these squared differences for i from 1 to n.
- $\sqrt{\sum_{i=1}^{n}(x_i - y_i)^2}$Finally, the square root of the sum of these squared differences is taken.

3.3 Assessment Methodology

Predictive models' accuracy and dependability are critical in determining their feasibility for real-world applications. A quantitative assessment of the correctness of predicted data becomes necessary in the field of stress distribution prediction to examine the robustness of the suggested technique. This assessment is aided by using the Root Mean Square Error (RMSE), a well-known statistic that provides a thorough insight into the model's prediction capabilities. As shown in the equation below, the RMSE quantifies the average size of deviations between predicted and actual values, producing a single result that incorporates the model's overall accuracy. The RMSE is calculated by taking the square root of the mean of squared errors as stated in Equation 3, which provides information on the amount and spread of mistakes throughout the dataset. This statistic, in addition to capturing trends and patterns, identifies occasions when forecasts deviate significantly from actual results. The practical relevance of RMSE is highlighted in assessing the accuracy of stress distribution estimates derived from the combined method, including FEA and ML-driven models, as discussed in the next section of this inquiry. The goal is to create a quantitative benchmark that captures the congruence between planned and actual stress distribution data while leveraging the effectiveness of RMSE. The results of this evaluative measure are critical in evaluating the usefulness of the proposed technique and offering insight into its potential to improve stress prediction accuracy in wind tunnel simulations.

$$RMSE = \sqrt{\frac{1}{m}\sum_{i=1}^{m}(x_i - y_i)^2} \times 100 \quad (3)$$

4. Results and Discussion

4.1 FEA utilizing fluid flow fluent and static structural

A comprehensive study was conducted to delve into the pressure and velocity distribution experienced by the aircraft prototype model within the wind tunnel, aiming to understand the intricate fluid dynamics showcased by the ANSYS Fluent simulations. As depicted in Figure 5, these findings provide a visual glimpse into the complex interplay of airflow. Notably, despite the initially low input velocity, the results reveal a delicate tapestry of varying velocity magnitudes enveloping the surface of the prototype model within the wind tunnel's confines in Figure 5 a. This velocity pattern exhibits a range from 1 to 12m/s² as

depicted in Figure 5 b, showing the profound influence of the intricate turbulence dynamics that unfold throughout the 3-meter wind tunnel. This nuanced range underscores the intricate nature of the aerodynamic environment, capable of generating dynamic flow characteristics even when set in motion by modest initial velocities. Furthermore, the visualization of flow pressure distribution during the wind tunnel simulation presents a pressure spectrum ranging from 0.2 Pa to 5 Pa. These quantified pressure variations are tangible evidence of the dynamic aerodynamic forces in the simulation setup. These fluctuating pressure gradients confirm the significance of fluid flow dynamics on the aircraft prototype model and underscore the necessity of considering these intricate interactions when evaluating stress distribution. The ANSYS Fluent simulations unveil a captivating dance between velocity and pressure distributions, emphasizing the intricate nature of the aerodynamic surroundings within the wind tunnel. This array of results underscores the vital importance of in-depth fluid flow analyses when unraveling the mechanical behavior of the aircraft prototype model during the testing phase.

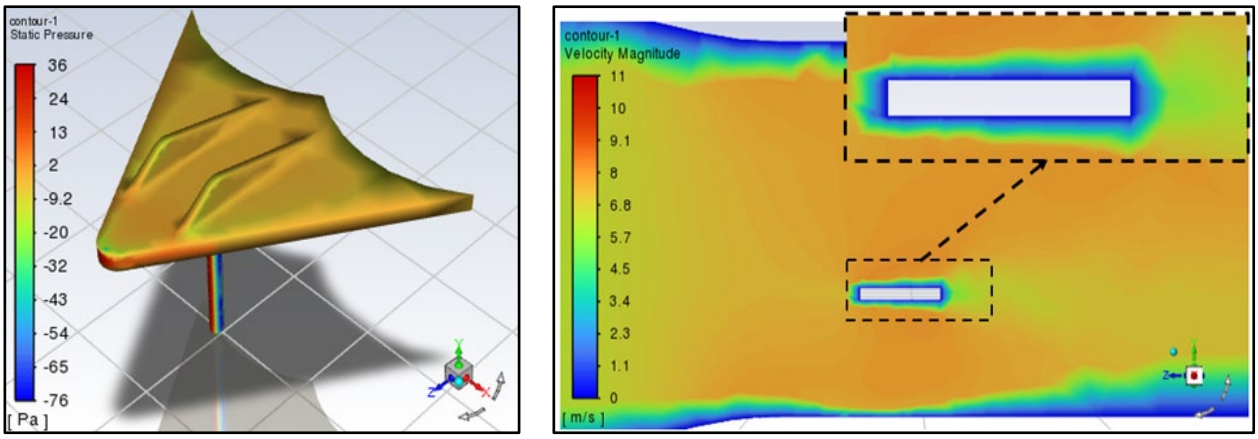

(a) **(b)**

Figure 5: Fluid flow fluent simulation: (a) Static pressure, (b) velocity magnitude

Furthermore, the stress, measured in Pa, and the corresponding deformation in mm of the prototype's structure under static structural analysis are illustrated in Figure 6. The observed deformation in Figure 6b varies from 0.006 mm in the midsections to 0.012 mm in the front and back sections. On the other hand, stress in Figure 6a ranges from 1000 Pa in the front and back sections to 5000 Pa in the midsection. These findings lay the groundwork for the subsequent discussion, which delves into integrating the fluid flow data into the comprehensive framework of FEA and ML-driven models, with the overarching aim of refining stress distribution predictions.

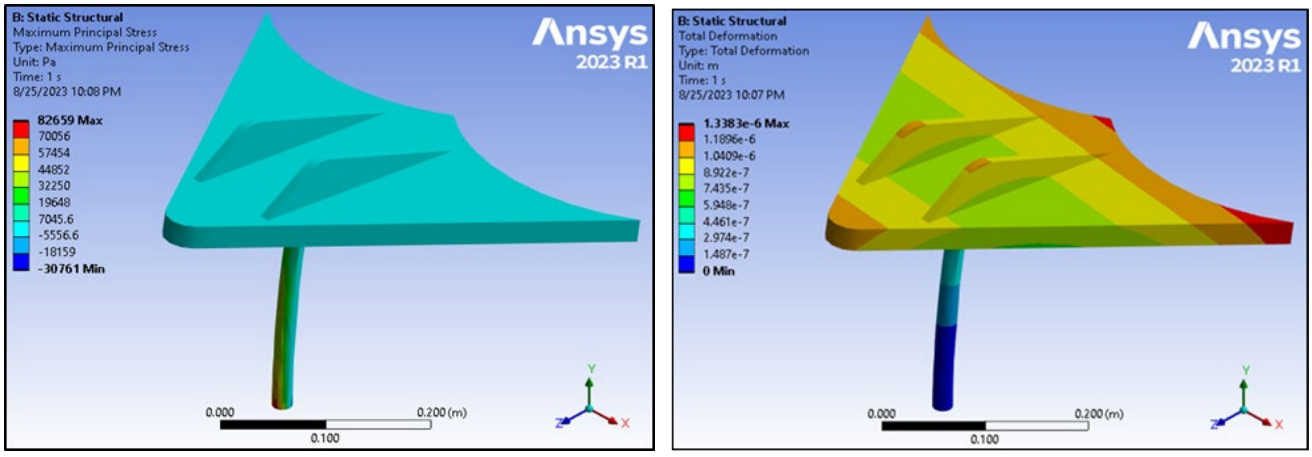

(a) (b)

Figure 6: Static structural: (a) Stress distribution; (b) Deformation

4.2 ML-driven based models utilizing SVM and kNN

Table 3 compares real stress levels to stress predictions produced from the SVM and kNN regression models. Where the models solely depend on the trained values of FEA of a signal run, and the rest is forecasted depending on the ML-based models. These forecasts are derived using an integrated approach that blends FEA with machine learning methods to improve stress distribution projections for the aircraft model's front wing during wind tunnel simulations. The processing time needed for these predictions is a significant feature of this comparison. Compared to standard FEA computations, the SVM and kNN models perform well. Notably, the FEA study took roughly 2 hours to calculate the stress distribution for the provided aircraft span values. On the other hand, the SVM model finished the stress prediction procedure in only 10 seconds, while the kNN model was even quicker, taking just 3 seconds. This large difference in computing time highlights ML-driven models' computational

edge, giving them a more time-efficient choice for stress distribution forecasts. Returning to the stress predictions, the actual stress levels vary from 1022 Pa to 4899 Pa across various span values, representing variances in the stress encountered by the aircraft model's front wing inside the wind tunnel. We see a remarkable agreement with the real stress levels when we examine the SVM-predicted stress levels. For instance, for a span of 0.1 m, the actual stress is 3035 Pa, which is quite similar to the SVM-predicted stress of 3025.84 Pa. This degree of concordance demonstrates the SVM model's ability to effectively capture stress patterns. The kNN forecasts, on the other hand, show minimal differences from the actual stress levels. The real stress is 2050 Pa at a span value of 0.05 m, whereas the kNN-predicted stress is 2132.35 Pa. These little differences show the complexities of stress prediction using kNN and the difficulty in capturing subtle stress fluctuations. Adding numbers for Root Mean Square Error (RMSE) offers a quantitative measure of prediction accuracy. The RMSE of the SVM model is 2.1%, suggesting an average variation of around 2.1% from real stress levels. In contrast, the RMSE of the kNN model is 5.6%, showing a significantly greater margin of error. These RMSE figures verify the SVM model's improved accuracy in stress prediction for the aircraft's front wing.

In conclusion, Table 3 highlights the promise of the combined FEA-SVM and FEA-kNN techniques in stress prediction and the efficiency of machine learning-driven models. The substantial decrease in computing time, with SVM and kNN models completing predictions in seconds, demonstrates these models' computational superiority over conventional FEA approaches. This demonstrates the effectiveness of integrating Finite Element Analysis and machine learning approaches to improve stress distribution estimates while greatly shortening the prediction process.

Table 2: Stress distribution and predictions

Aircraft span value (m)	Stress (Pa)	SVM Predicted Stress (Pa)	kNN Predicted Stress (Pa)
0	1022	1003.73	968.51
0.05	2050	2058.49	2132.35
0.1	3035	3025.84	3199.29
0.2	4233	4252.62	3981.52
0.25	4899	4893.76	5137.23
0.3	4230	4218.11	4409.94
0.4	3032	3034.76	3225.61
0.45	2052	2049.66	2134.79
0.5	1025	1030.55	1028.56

Figure 7 visually represents the results reported in the previous table, visually explaining stress distribution patterns throughout the aircraft model. Figure 7 a depicts stress lines crossing the model's span in three dimensions. In contrast, Figure 7 b illustrates a front-view projection of this three-dimensional viewpoint, allowing for a more in-depth investigation of the stress distribution. A strong alignment is shown in the graphical depiction between the blue line indicating real stress levels determined from FEA-based analysis and the orange line showing SVM-based stress predictions. This remarkable concordance strengthens the SVM regression model's accuracy, which is especially attractive given its capacity to produce quick forecasts in seconds. The SVM model's temporal efficiency becomes a notable benefit, proving its dependability and applicability. Furthermore, the kNN regression model performs well, with stress predictions that nearly match the actual stress levels. Although somewhat less accurate than the SVM model, the kNN predictions maintain a noteworthy accuracy. Notably, the kNN model's appropriateness for improving static structural analysis of wind tunnel-affected airfoil models is still apparent, bolstering its prospective contributions to engineering simulations.

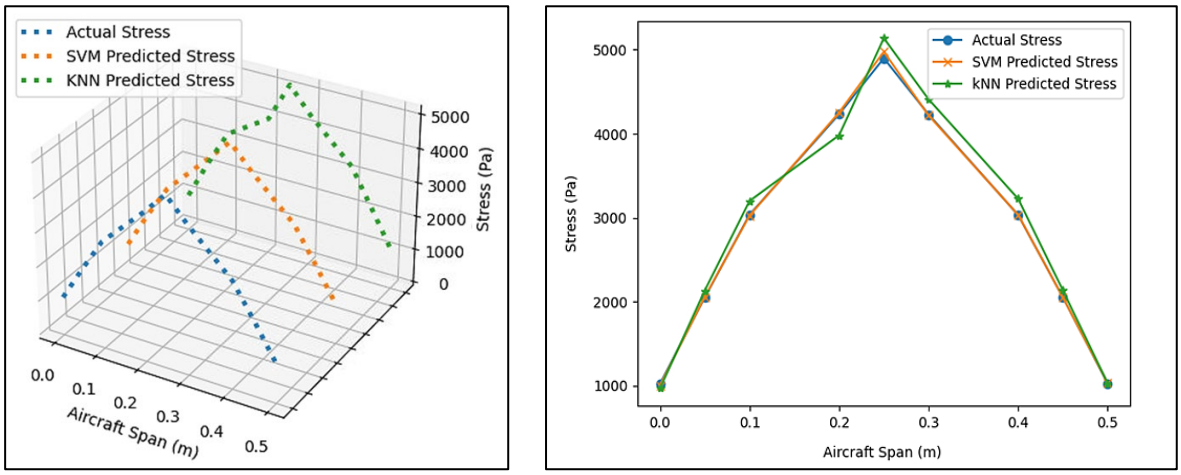

Figure 7: Machine learning-based models' assessment: (a) 3D View of the actual and two prediction models; (b) 2D front view of the actual and two prediction models

5. Conclusion

This study introduced an extensive methodology to enhance stress distribution predictions in wind tunnel computational simulations for aircraft models. The approach entails the integration of FEA with SVM and kNN regression models, yielding accurate and efficient forecasts. The investigation meticulously examines ANSYS Fluent findings, unveiling intricate fluid dynamics within the wind tunnel. Subsequently, the SVM and kNN regression models are introduced, showcasing their proficiency in stress distribution forecasting by deciphering complex data patterns. The comparative analysis of stress projections, accompanied by the RMSE, underlines the proposed methodology's efficacy. Notably, the SVM model demonstrated exceptional accuracy, reflecting its 2.1% RMSE, surpassing the kNN model with a 5.6% RMSE. Importantly, the stress distribution calculations using FEA took approximately 2 hours, whereas SVM and kNN required only 10 seconds and 3 seconds, respectively, underscoring the significant time-saving attributes of these models. Overall, the computational efficiency of SVM and kNN is highlighted, emphasizing their adaptability in stress analysis. This comprehensive approach ushers in a promising trajectory in engineering simulations, enabling precise stress distribution forecasts essential for advancing aircraft design methodologies and refining wind tunnel evaluations.

Author contributions

Conceptualization, L. Al-Haddad, A. Jaber, L. Ibraheem, S. Al-Haddad, N. Ibrahim and F. Abdulwahed; methodology, A. Jaber and S. Al-Haddad; software, N. Ibrahim and F. Abdulwahed; validation, L. Al-Haddad and S. Al-Haddad; formal analysis, L. Al-Haddad; investigation, L. Al-Haddad; writing—original draft preparation, L. Al-Haddad; writing—review and editing, L. Al-Haddad, A. Jaber and L. Ibraheem. All authors have read and agreed to the published version of the manuscript.

Funding

This research received no specific grant from any funding agency in the public, commercial, or not-for-profit sectors.

Data availability statement

The researcher took the information, and the rest of the data is in the author's thesis in the Department of Mechanical Engineering, University of Technology library.

Conflicts of interest

The authors declare that there is no conflict of interest.

References

[1] L. A. Al-Haddad, An Intelligent Fault Diagnosis Approach for Multirotor UAVs Based on Deep Neural Network of Multi-Resolution Transform Features, Drones, 7 (2023) 82 .https://doi.org/10.3390/drones7020082

[2] L. A. Al-Haddad, A. A. Jaber, P. Neranon, S. A. Al-Haddad, Investigation of Frequency-Domain-Based Vibration Signal Analysis for UAV Unbalance Fault Classification, Eng. Technol. J., 41 (2023) 915-923. https://doi.org/10.30684/etj.2023.137412.1348

[3] Z. Cui, G. lai, WANG, Q. LIANG, Y. and CAO, Y., Wind Tunnel Investigation of Different Engine Layouts of a Blended-Wing-Body Transport, Chinese J. Aeronaut., 36 (2023) 123-132. https://doi.org/10.1016/j.cja.2023.04.027

[4] M. F. Westin, J. M. Balthazar, R. G. A. da Silva, Ribeiro, M. A. Tusset, Characterization of Aeroelastic Behavior in a High Aspect Ratio Wing Using Computational and Wind Tunnel Experiments, Axioms, 12 (2023). https://doi.org/10.3390/axioms12090826

[5] J. Smolka, K. Kempná,P. Kučera, K. Kempný, E. Asimakopoulou, P. Danihelka, Setup of a 3D Printed Wind Tunnel: Application for Calibrating Bi-Directional Velocity Probes Used in Fire Engineering Applications, HardwareX, 15 (2023) e00440. https://doi.org/10.1016/j.ohx.2023.e00440

[6] C. Zhiming, F. XUE, H. YU, Y. WANG, Z. JIANG, W. LU, L. DONG, Derivation and Validation of a Similarity Law for Free-Flight Wind Tunnel Tests of Parallel Stage Separation, Chinese J. Aeronaut., 36 (2023) 91–100. https://doi.org/10.1016/j.cja.2023.02.010

[7] W. Li, W. Zou, J. Fu, F. Gao, M. Yu, Development of an Anti-Vibration Aircraft Model Support System with Magnetorheological Annular Squeeze Dampers for Wind Tunnel, Mech. Syst. Signal Process., 202 (2023) 110663. https://doi.org/10.1016/j.ymssp.2023.110663

[8] L. A. Al-Haddad, A. A. Jaber, Influence of Operationally Consumed Propellers on Multirotor UAVs Airworthiness: Finite Element and Experimental Approach, IEEE Sensors J., 23 (2023) 11738-11745. https://doi.org/10.1109/JSEN.2023.3267043

[9] S. S. Shijer, Simulation of Piezoelectric in Engine Knock Sensor with Different Frequency Modes, ECS Transactions, 107 (2022) 17271. https://doi.org/10.1149/10701.17271ecst

[10] A. A. Dubaish, A. A. Jaber, Fabrication of a Test Rig for Gearbox Fault Simulation and Diagnosis, Diagnostyka, 24 (2023) 2023204. https://doi.org/10.29354/diag/162541

[11] N. Yassa, M. Rachek, Modeling and Detecting the Stator Winding Inter Turn Fault of Permanent Magnet Synchronous Motors Using Stator Current Signature Analysis, Math Comput Simul, 167 (2020) 325–39. https://doi.org/10.1016/j.matcom.2018.04.012

[12] L. A. Al-Haddad, A. A. Jaber, S. A. Al-Haddad, Y. M. Al-Muslim, Fault Diagnosis of Actuator Damage in UAVs Using Embedded Recorded Data and Stacked Machine Learning Models, J. Supercomput., (2023). https://doi.org/10.1007/s11227-023-05584-7

[13] P. Casabianca, Y. Zhang, Acoustic-Based UAV Detection Using Late Fusion of Deep Neural Networks, Drones, 5 (2021). https://doi.org/10.3390/drones5030054

[14] X. Xiaoqian, A Sensor Fault Diagnosis Algorithm for UAV Based on Neural Network, 2021 Int. Conf. Intell. Transp., Big Data & Smart City, Xi'an, China, (2021) 260–65. https://doi.org/10.1109/ICITBS53129.2021.00072

[15] M. Moussafir, H. Chaibi, R. Saadane, A. Chehri, A. El Rharras, G. Jeon, Design of Efficient Techniques for Tomato Leaf Disease Detection Using Genetic Algorithm-Based and Deep Neural Networks, Plant Soil, 479 (2022) 251–266. https://doi.org/10.1007/s11104-022-05513-2

[16] A. A. F. Ogaili, M. N. Hamzah, A. A. Jaber, Integration of Machine Learning (ML) and Finite Element Analysis (FEA) for Predicting the Failure Modes of a Small Horizontal Composite Blade, Int. J. Renew. Energy Res., 12 (2022) 2168–2179.

[17] E. H. Flaieh, F. O. Hamdoon, A. A. Jaber, Estimation the Natural Frequencies of a Cracked Shaft Based on Finite Element Modeling and Artificial Neural Network, Int. J. Adv. Sci. Eng. Inf. Technol., 10 (2020) 1410–16.

[18] C. Kuang-Hua, E-Design: Computer-Aided Engineering Design, Academic Press, 2016.

[19] L. Yuan, D. Lian, X. Kang, Y. Chen, and K. Zhai, Rolling Bearing Fault Diagnosis Based on Convolutional Neural Network and Support Vector Machine, IEEE Access, 8 (2020) 137395–137406. https://doi.org/10.1109/ACCESS.2020.3012053

[20] Al-Mukhtar, M., Modeling the Monthly Pan Evaporation Rates Using Artificial Intelligence Methods: A Case Study in Iraq, Environ. Earth Sci., 80 (2021). https://doi.org/10.1007/s12665-020-09337-0

[21] M. Al-Mukhtar, Random Forest, Support Vector Machine, and Neural Networks to Modelling Suspended Sediment in Tigris River-Baghdad, Environ. Monit. Assess., 191 (2019). https://doi.org/10.1007/s10661-019-7821-5

[22] M. A. Jamil, M. A. A. Khan , S. Khanam, Feature-Based Performance of SVM and KNN Classifiers for Diagnosis of Rolling Element Bearing Faults, Vibroengineering Procedia, 39 (2021) 36–42. https://doi.org/10.21595/vp.2021.22307

[23] L. A. Al-Haddad, A. A. Jaber, Improved UAV Blade Unbalance Prediction Based on Machine Learning and ReliefF Supreme Feature Ranking Method, J. Braz. Soc. Mech. Sci. Eng., 45 (2023b) 463. https://doi.org/10.1007/s40430-023-04386-5